

Hydrodynamic Trapping of Tracer Particles Induced by Spatially Correlated Noise in Thermal Equilibrium

Sijie Huang (黄斯杰),^{1,2} Ayush Saurabh,^{1,2} and Steve Presse^{1,2,3,*}

¹Department of Physics, Arizona State University, Tempe, AZ 85287, USA

²Center for Biological Physics, Arizona State University, Tempe, AZ 85287, USA

³School of Molecular Sciences, Arizona State University, Tempe, AZ 85287, USA

(Dated: July 14, 2025)

We investigate the fluctuating Stokes equation in the presence of spatially correlated noise—characterized by a single length scale—while preserving thermal equilibrium through the corresponding fluctuation-dissipation relation. Numerical simulations reveal that a tracer particle’s mean-squared displacement (MSD) depends nonmonotonically on the ratio ℓ/r between the correlation length ℓ and the particle radius r : the MSD decreases as ℓ approaches r , reaches a minimum near $\ell \simeq r$, and rises again for $\ell > r$. The initial suppression stems from transient trapping, where sluggish momentum diffusion at short wavelengths confines the particle. When $\ell > r$, the particle hops between traps and eventually recovers normal diffusion ($\text{MSD} \propto t$) consistent with the fact that momentum diffusion crosses over to the standard Laplacian at long wavelengths. We further illustrate that spatial correlation introduces nonlocal momentum diffusion in the hydrodynamic equations, reminiscent of the slow dynamics in glassy and other disordered systems.

Deviation from linear time scaling of the mean-squared displacement (MSD) predicted by Brownian motion, termed anomalous diffusion, is encountered across a range of fields [1–3]. Such anomalous diffusion is often associated with nonequilibrium settings—such as active matter, biological cells, and systems driven by external forces or energy-consuming processes—where continuous energy input or active forces are essential [4, 5]. Spatial correlations, a hallmark of nonequilibrium dynamics, emerge spontaneously in these systems, *e.g.*, in hydrodynamic turbulence [5–7]. On the other hand, equilibrium systems can also exhibit anomalous diffusion. This is true despite the absence of energy input or external driving in these systems and has been attributed to spatial heterogeneities (*e.g.*, geometric constraints, spatial confinement, disordered or fractal structures) or memory effects intrinsic to the medium (*e.g.*, viscoelasticity) [8–10].

In the context of fluctuating hydrodynamics, intrinsic thermal fluctuations are represented by a stochastic stress tensor modeled by delta-correlated noise in space and time; a fluid driven by this stochastic forcing faithfully reproduces the classic Brownian diffusion of immersed particles [11, 12]. In contrast, anomalous diffusion may arise within a fluctuating hydrodynamic framework by considering spatial correlations. Indeed, under equilibrium conditions, anomalous diffusion induced by spatial heterogeneities or confinement is often modeled by external spatial correlations [13, 14].

In this Letter, we introduce spatially correlated thermal fluctuations, characterized by a single correlation length, ℓ , and sufficiently rapid decay (as opposed to algebraic long-range correlations). We derive the corresponding fluctuation-dissipation relation (FDR), thereby altering the fluid’s momentum diffusion, which becomes nonlocal. Nonlocal dynamics have been widely employed in modeling diverse biological systems, including animal and cellular population dynamics [15]. The resulting nonlocality resembles the structure of the McKean–Vlasov equation, wherein the correlation function is replaced by an interaction potential describing in-

terparticle attraction and aggregation [16, 17]. The resulting nonlocality renders hydrodynamic momentum diffusion scale-dependent, leading to a nonmonotonic dependence of the particle’s MSD on the ratio ℓ/r of correlation length ℓ to particle radius r : the MSD decreases with increasing ℓ/r , attains a minimum near $\ell \simeq r$, and rises again for larger ratios. The initial drop arises from suppressed short-wavelength momentum diffusion, which transiently traps the particle. As ℓ exceeds r , the particle hops through a network of such traps. In this regime, the fluid’s momentum diffusion crosses over to the standard Laplacian, and the particle motion returns to normal diffusion ($\text{MSD} \propto t$). Moreover, we demonstrate that the system dynamics and anomalous transport share some similarities with the slow dynamics observed in disordered media such as glasses, revealing a link between equilibrium correlated hydrodynamics and glassy-like systems.

Formulation.—At the continuum level, thermally fluctuating fluids can be described by the fluctuating incompressible linearized Navier–Stokes (*i.e.*, Stokes) equation, originally introduced by Landau and Lifshitz [18], formulated as

$$\partial_t \mathbf{u} = -\nabla p + \nu \nabla^2 \mathbf{u} + \sqrt{2\nu k_B T \rho^{-1}} \nabla \cdot \mathcal{W}, \quad (1)$$

where \mathbf{u} and p are the fluid velocity and mechanical pressure, respectively. Thermodynamic quantities—density ρ , kinematic viscosity ν , and temperature T —are all assumed constant. This equation describes a coarse-grained velocity field on length scales larger than the mean free path of the underlying fluid molecules [19]. The stochastic momentum flux is modeled via a spatiotemporal white Gaussian random tensor, $\mathcal{W}(\mathbf{x}, t)$, with covariance determined by a FDR [20]

$$\begin{aligned} \langle \mathcal{W}_{ij}(\mathbf{x}, t) \mathcal{W}_{lm}(\mathbf{x}', t') \rangle &= (\delta_{il} \delta_{jm} + \delta_{im} \delta_{jl}) \\ &\times \delta(\mathbf{x} - \mathbf{x}') \delta(t - t'). \end{aligned} \quad (2)$$

Velocity fluctuations driven by the noise in Eq. (2) span a wide range of spatial scales in Eq. (1). The FDR ensures that, at each length scale, the energy injected by the noise is balanced by viscous dissipation, thereby maintaining thermal equilibrium.

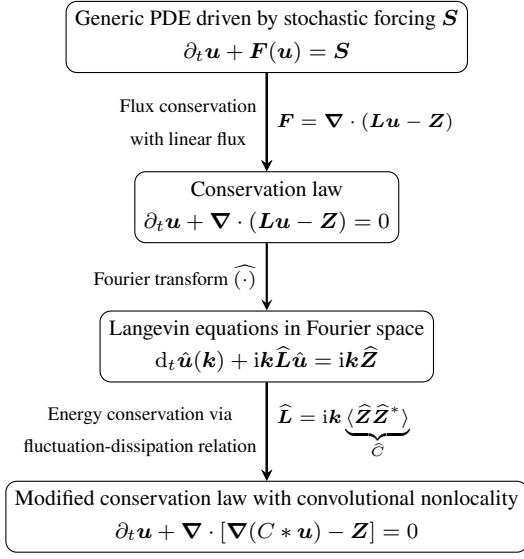


FIG. 1. Schematic derivation of our spatially correlated expression under increasingly stringent physical constraints, culminating in a nonlocal conservation law. From a generic noise-driven equation, imposing flux conservation and linearity recovers the standard fluctuating Stokes equation. Introducing spatially correlated noise and enforcing the fluctuation-dissipation relation in Fourier space yields a modified conservation law, whose physical-space form is nonlocal due to a convolution kernel.

Here, we extend Eq. (1) to spatially correlated, temporally white noise $\mathbf{Z}(\mathbf{x}, t)$ with covariance

$$\langle \mathbf{Z}_{ij}(\mathbf{x}, t) \mathbf{Z}_{lm}(\mathbf{x}', t') \rangle = (\delta_{il}\delta_{jm} + \delta_{im}\delta_{jl}) \times C_\ell(|\mathbf{x} - \mathbf{x}'|) \delta(t - t'), \quad (3)$$

where the isotropic correlation function $C_\ell(|\mathbf{x} - \mathbf{x}'|)$ is characterized by a single length scale ℓ . In the white-noise limit $\ell = 0$, we set $C_\ell(|\mathbf{x} - \mathbf{x}'|) = \delta(|\mathbf{x} - \mathbf{x}'|)$; $\mathbf{Z}(\mathbf{x}, t)$ then reduces to the uncorrelated field $\mathbf{W}(\mathbf{x}, t)$.

Considering the spatial Fourier transform of Eq. (1), for uncorrelated noise, the energy injected into each Fourier mode scales as k^2 , consistent with the standard Laplacian operator. Introducing spatial correlations in the noise modifies the k^2 scaling, redistributing the energy injection across different spatial scales. To retain the energy input-output balance—and hence maintain thermal equilibrium—the momentum diffusion term must be adjusted in accordance with the chosen correlation function, analogous to the memory kernel arising in the generalized Langevin equation derived from the Mori–Zwanzig projection formalism [21–23].

The required alteration to the momentum diffusion term is easily carried out in Fourier space. Here we provide a summary; see Sec. I of the Supplemental Material [24] for further details. Figure 1 sketches the derivation of the generalized equation driven by spatially correlated noise that satisfies the FDR. In Fourier space, the fluctuating Stokes equation can be expressed as a linear system of decoupled Langevin equations

$$\frac{d}{dt} \hat{\mathbf{u}}(\mathbf{k}) = \mathcal{L}(\mathbf{k}) \hat{\mathbf{u}} + i\sqrt{2\nu k_B T \rho^{-1}} \mathcal{P} \mathbf{k} \cdot \hat{\mathbf{Z}}, \quad (4)$$

where $\mathcal{L}(\mathbf{k})$ is the linear momentum diffusion operator, and the incompressibility constraint is enforced by the Leray projection operator $\mathcal{P} = \mathbf{I} - \mathbf{k}\mathbf{k}^\top/k^2$. This equation is analogous to the generalized Langevin equation for electron-phonon coupling proposed in Ref. [25], which likewise incorporates spatially correlated driving noise. We can solve each Fourier mode individually, and the resulting covariance for the modes at equilibrium is given by

$$\langle \hat{\mathbf{u}}(\mathbf{k}) \hat{\mathbf{u}}^\dagger(\mathbf{k}) \rangle = -\frac{\nu k_B T}{\rho} \frac{k^2 \hat{\mathbf{C}}_\ell(\mathbf{k})}{\mathcal{L}}, \quad (5)$$

where the superscript \dagger denotes Hermitian conjugate. Substituting the Laplacian $\mathcal{L}(\mathbf{k}) = -\nu k^2$ and the delta correlation function $C_\ell = \delta$ into Eq. (5) and taking the trace yields the total kinetic energy of the Fourier mode

$$\langle |\hat{\mathbf{u}}|^2 \rangle = (d-1) \frac{k_B T}{\rho}, \quad (6)$$

where d denotes the spatial dimension. The prefactor $d-1$ follows directly from $\text{Tr}(\mathcal{P})$; by enforcing incompressibility, the projection operator \mathcal{P} removes one degree of freedom and its associated share of thermal energy [26]. Accordingly, Eq. (6) predicts equipartition of energy among all Fourier modes.

The linear diffusion operator corresponding to the correlated noise follows directly by equating the trace of Eq. (5) to Eq. (6), yielding

$$\mathcal{L}(\mathbf{k}) = -\nu k^2 \hat{\mathbf{C}}_\ell(\mathbf{k}). \quad (7)$$

The correlation function $\hat{\mathbf{C}}_\ell(\mathbf{k})$ explicitly appears in the diffusion operator Eq. (7), modulating momentum diffusion strength in Fourier space to ensure scale-wise energy equilibrium. Inserting into Eq. (4) the explicit form given by Eq. (7) and transforming back into physical space, the fluctuating Stokes equation driven by the spatially correlated noise is expressed as

$$\partial_t \mathbf{u} = -\nabla p + \nu \nabla^2 \tilde{\mathbf{u}} + \sqrt{2\nu k_B T \rho^{-1}} \nabla \cdot \mathbf{Z}, \quad (8)$$

where $\tilde{\mathbf{u}}(\mathbf{x}) = \int C_\ell(\mathbf{x}') \mathbf{u}(\mathbf{x} - \mathbf{x}') d\mathbf{x}'$ is the correlated velocity. The convolution in the diffusive flux indicates that fluid momentum diffusion is explicitly nonlocal, arising through the convolution of the correlation function with fluid velocity. Such a convolutional nonlocality, as previously pointed out, also appears in the McKean–Vlasov equation.

Results.—To investigate diffusion of tracer particles in fluid flows governed by Eq. (8), we numerically solve the coupled fluid-particle system. Particles are treated as passive and inertialess, advected by the fluid flow, without exerting forces back on the fluid. Simulations employ the inertial coupling method developed in Refs. [27, 28]; further simulation details are provided in Sec. II of the Supplemental Material [24]. Briefly, the fluid-particle system is solved in a doubly periodic domain of side length $2\pi \mu\text{m}$ for particles of size $r = 0.1 \mu\text{m}$. Equation (8) is transformed to Fourier space and integrated in

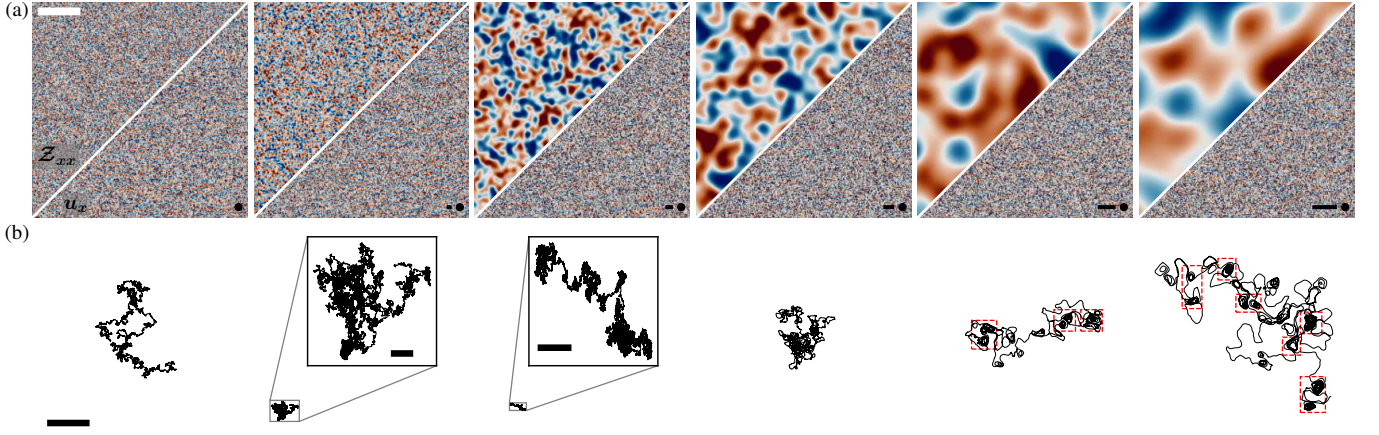


FIG. 2. Evolution from ordinary Brownian motion to hydrodynamic trapping as the noise correlation length ℓ grows relative to the particle radius $r = 0.1 \mu\text{m}$. (a) Instantaneous fields of the correlated noise (upper halves) and the resulting fluid velocity (lower halves) for $\ell/r = 0, 1/4, 1, 2, 4$, and 6 (left to right). Only the components in the x -direction are shown (Z_{xx} and u_x) thanks to spatial isotropy. A black disk and adjacent line indicate the particle size and the corresponding correlation length, respectively; white bar, $1 \mu\text{m}$. (b) Representative tracer trajectories over the same time span; black bar, $1 \mu\text{m}$; inset bars, $0.1 \mu\text{m}$. Red boxes on the right-hand side for $\ell/r = 4$ and 6 highlight episodes of transient trapping. Simulation methods and parameters are described in Sec. II and summarized in table I of the Supplemental Material [24].

time using the Crank–Nicolson method [29], whereas particle trajectories are updated using a midpoint predictor-corrector scheme [28]. The correlation function is assumed to be Gaussian, $C_\ell(|\mathbf{x} - \mathbf{x}'|) = \exp[-|\mathbf{x} - \mathbf{x}'|^2/(2\ell^2)]$, for finite correlation length $\ell > 0$; for $\ell = 0$, the Gaussian correlation is replaced by the delta function $\delta(|\mathbf{x} - \mathbf{x}'|)$. We examine six values of the correlation length-to-particle radius ratio, $\gamma \equiv \ell/r = 0, 1/4, 1, 2, 4$, and 6 . Validation tests are provided in Sec. III of the Supplemental Material [24]. Figure 1 of the Supplemental Material shows flat Fourier energy spectra—evidence of mode-by-mode equipartition—and velocity probability distributions consistent with the equilibrium Boltzmann distribution for all values of γ . Figure 2 confirms that, under uncorrelated noise ($\gamma = 0$), particle diffusion reproduces the expected Brownian behavior.

Figure 2(a) shows examples of instantaneous fluid velocity component in the x -direction, u_x , driven by the noise with six different correlation lengths. In the case of uncorrelated noise ($\gamma = 0$), the velocity field appears spatially random without discernible structures, consistent with thermal equilibrium, in which energy is evenly distributed across scales. In contrast, correlated noise produces large-scale structures with characteristic sizes set by the correlation length; however, even in this case, the absence of persistent spatial structures indicates that the fluid remains at thermal equilibrium.

Representative trajectories of the particles are first shown in Fig. 2(b) for visual purposes while quantitative analysis later appears in Fig. 4. As already seen visually from their trajectories, particle diffusion exhibits a nonmonotonic behavior with respect to the ratio γ of noise-correlation length to particle radius. With uncorrelated noise ($\gamma = 0$), the trajectory appears irregular and erratic, characteristic of anticipated evolution under Brownian motion. As γ approaches unity, the particle diffuses more slowly, yet its motion remains Brownian, as

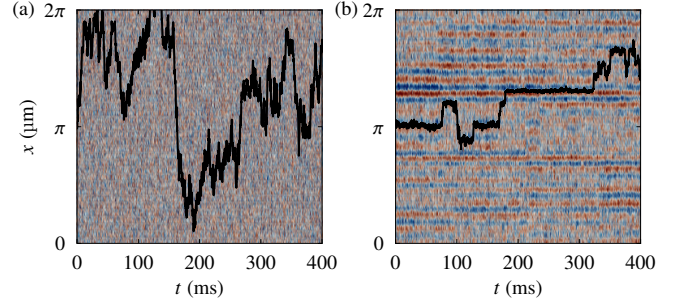


FIG. 3. Comparison of 1D particle trajectories in uncorrelated- and correlated-noise cases. Space-time contours of the 1D velocity field driven by spatially (a) uncorrelated and (b) correlated noise, with representative particle trajectories overlaid (black solid lines). Trajectory in the correlated-noise case exhibits markedly long residence times (trapping), in contrast to particles evolving under standard Brownian diffusion. Simulation parameters are the same as Fig. 1.

the MSD shown below confirms. When $\gamma > 1$, the diffusion rate rises again and the trajectory becomes smoother and more persistent, with fewer abrupt turns. For $\gamma \geq 2$, the particle undergoes transient hydrodynamic trapping: the path threads a network of well-separated traps and, at larger γ 's, the particle hops between them. In this limit, the long-time MSD reverts to effectively normal diffusion, as shown later (Fig. 4). As the fluid flow is spatially homogeneous and isotropic, any particle trapping must arise from its spatial correlation. Considering the Gaussian correlation model allows us to provide mechanistic insight: at small scales, momentum relaxes slowly, creating temporary traps, whereas at larger scales, momentum diffusion follows the ordinary Laplacian. As such, the motion ultimately crosses over to standard Brownian diffusion.

To provide a more intuitive illustration of particle trapping,

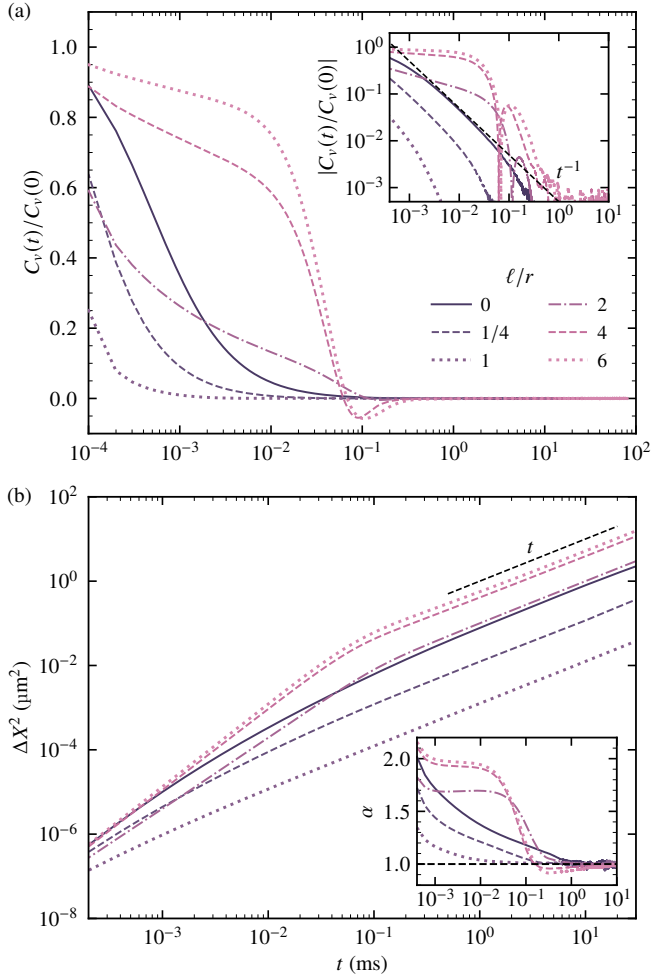


FIG. 4. Particle VACF and MSD exhibit nonmonotonic dependence on the dimensionless ratio γ . (a) Normalized VACF, and (b) MSD ΔX^2 . Insets in (a) show the absolute value of the VACF on a log-log scale, and in (b) the local slope α of ΔX^2 . As γ increases, the MSD initially decreases and then rises, whereas the VACF remains Brownian-like for $\gamma \leq 1$ but develops complex dynamical features for $\gamma > 1$ described in the main text. Simulation parameters are the same as Fig. 1.

we examine particle diffusion in one dimension, where the fluctuating Stokes equation [Eq. (8)] reduces to a stochastic diffusion equation. As shown in Fig. 3(a), the velocity field driven by the uncorrelated noise remains featureless. A representative trajectory under correlated noise, shown in Fig. 3(b), exhibits a pronounced staircase-like time trace with extended residence intervals, in stark contrast to the irregular, structureless wander under uncorrelated noise. This behavior is consistent with our 2D findings, suggesting that trapping arises from genuine noise correlations and fundamentally alters the particle's diffusive transport.

To characterize the diffusion process quantitatively, we calculated the particle velocity autocorrelation function (VACF), defined as $C_v(t) = \langle v(\tau)v(\tau+t) \rangle$, where $v(t)$ is the particle velocity. The results are shown in Fig. 4(a). For uncorre-

lated noise, the VACF initially decays rapidly, indicating quick decorrelation from its initial velocity. It then transitions to the hydrodynamic regime, exhibiting the classical t^{-1} scaling in two dimensions [Fig. 4(a), inset], resulting from the hydrodynamic memory effect due to momentum conservation [32, 33].

As γ increases to unity, the overall shape of the VACF remains largely unchanged, except for a more rapid short-time roll-off. This behavior suggests that the spatial correlation suppresses the initial ballistic regime, facilitating the transition to the normal diffusive regime. This also explains the slower diffusion observed in Fig. 2(b).

For $\gamma > 1$, the VACF evolves through successive stages. Following the same rapid initial drop observed at $\gamma < 1$, the VACF enters a slower, nearly linear decay for $10^{-3} < t < 10^{-1}$ ms. Around $t \simeq 10^{-1}$ ms, the curve crosses the origin and develops a negative minimum, appearing first at $\gamma = 2$ and deepening as γ further increases. The negative dip signals transient hydrodynamic trapping, which impedes normal diffusive transport of the particles.

While the VACF is useful in characterizing particle diffusion, it is equally interesting to investigate the particle position, and thus MSD, defined as $\Delta X^2(t) = \langle |\mathbf{X}(\tau+t) - \mathbf{X}(\tau)|^2 \rangle$, where $\mathbf{X}(t)$ is the particle position. Results for MSD as a function of time are shown in Fig. 4(b). Differences among the MSDs for different γ from 0 to 1 are evident only on short to intermediate time scales. Analysis of the local slope, $\alpha = d \ln \Delta X^2 / d \ln t$ [Fig. 4(b), inset], allows us to determine that normal diffusion ($\alpha = 1$) is restored for $t > 10$ ms. For the three cases where $\gamma \leq 1$, consistent with the observation made above, the ballistic regime is suppressed as γ increases from 0 to 1.

The MSD for $\gamma \geq 2$ reveals richer dynamical behaviors. Initially, for $t < 10^{-3}$ ms, the particles exhibit super-ballistic diffusion ($\alpha > 2$). Subsequently, for $10^{-3} < t < 10^{-2}$ ms, the MSD plateaus slightly around $\alpha = 2$ for a short period, suggesting quasi-ballistic motion. Thereafter, for $t > 10^{-2}$ ms, the MSD decreases until entering a subdiffusive trapping regime ($\alpha < 1$) for $t \gtrsim 10^{-1}$ ms, indicative of particle confinement. Ultimately, the trapping is temporary; at long times $t > 10$ ms, the MSD returns to the normal diffusive regime with $\alpha = 1$.

Discussion.—We have derived a fluctuating Stokes equation driven by spatially correlated noise that preserves thermal equilibrium. Particles diffusing in the resulting flow display transient, spatially intermittent trapping at large correlation lengths. Similar local confinement is observed in super-cooled glass-forming liquids, where dynamical heterogeneity slows the dynamics unevenly in space as the temperature approaches the glass transition: some regions relax rapidly, while others remain arrested, leading to particle trapping [8, 34–36].

The present system also exhibits dynamical heterogeneity—not in physical space, but in Fourier space. From Eq. (4), the linear diffusion operator $\mathcal{L}(\mathbf{k})$ acts as a damping coefficient for each Fourier mode, dictating its diffusion timescale $\tau_k \sim \mathcal{L}(\mathbf{k})^{-1}$. With uncorrelated noise, the ordinary Laplacian yields a uniform spectrum, $\tau_k \sim k^{-2}$, for all wavelengths.

Introducing a finite correlation length ℓ reshapes this spectrum: the timescale τ_k attains its minimum at $k_\ell \sim \ell^{-1}$, rises rapidly at shorter wavelengths $k \gg \ell^{-1}$, and recovers the ordinary Laplacian form—evident from a Taylor expansion of $\mathcal{L}(k)$ near $k = 0$ —at longer wavelengths $\ell^{-1} > k \simeq 1$. The resulting slowdown of momentum diffusion at short wavelengths produces transient particle trapping. In the long-time limit, momentum diffusion returns to the Laplacian regime, and particle motion crosses over to normal diffusion with $\text{MSD} \propto t$.

The extended diffusion timescales at large wavenumbers (k) signal sluggish dynamics of small-scale modes. The greater τ_k echoes the dramatic slowdown in glass-forming liquids, where structural relaxation times increase by many orders of magnitude as the temperature approaches the glass transition [37–39]. Here, however, the slowdown is dictated by spatial scale rather than elapsed time.

In the linearized (Stokes) regime we investigate here, Fourier modes remain uncoupled, *i.e.*, free from inter-mode interactions. Investigating the full nonlinear correlated fluctuating Navier–Stokes equation is a natural extension of the work presented here. In this equation, the nonlinear advection term couples the modes and will redistribute energy while conserving the total average energy, thereby preserving equilibrium [19]. This coupling is expected to redistribute energy from fast-diffusing modes to slower ones, thereby reshaping the short- and intermediate-time response, modifying the scale-dependent slow dynamics reported here, and possibly leading to particle dynamics and diffusion that differ from the present results.

This work was supported by the Army Research Office (ARO) under Grant No. W911NF-23-1-0304. Simulations were performed on the Sol cluster at Arizona State University.

* Corresponding author: spresse@asu.edu

- [1] I. C. Christov and H. A. Stone, Resolving a paradox of anomalous scalings in the diffusion of granular materials, *Proc. Natl. Acad. Sci. U.S.A.* **109**, 16012 (2012).
- [2] Z.-Q. Jiang, W.-J. Xie, W.-X. Zhou, and D. Sornette, Multifractal analysis of financial markets: a review, *Rep. Prog. Phys.* **82**, 125901 (2019).
- [3] G. M. Viswanathan, V. Afanasyev, S. V. Buldyrev, E. J. Murphy, P. A. Prince, and H. E. Stanley, Lévy flight search patterns of wandering albatrosses, *Nature* **381**, 413 (1996).
- [4] P. Dieterich, R. Klages, R. Preuss, and A. Schwab, Anomalous dynamics of cell migration, *Proc. Natl. Acad. Sci. U.S.A.* **105**, 459 (2008).
- [5] S. Mukherjee, R. K. Singh, M. James, and S. S. Ray, Anomalous diffusion and Lévy walks distinguish active from inertial turbulence, *Phys. Rev. Lett.* **127**, 118001 (2021).
- [6] L. F. Richardson, Atmospheric diffusion shown on a distance-neighbour graph, *Proc. R. Soc. Lond. A* **110**, 709 (1926).
- [7] C. Singh and A. Chaudhuri, Anomalous dynamics of a passive droplet in active turbulence, *Nat. Commun.* **15**, 3704 (2024).
- [8] F. Rusciano, R. Pastore, and F. Greco, Fickian non-Gaussian diffusion in glass-forming liquids, *Phys. Rev. Lett.* **128**, 168001 (2022).
- [9] A. D. Viñales, M. Camuyrano, and G. H. Paissan, Oscillations and negative velocity autocorrelation emerging from a Brownian particle model with hydrodynamic interactions, *Phys. Rev. E* **101**, 052140 (2020).
- [10] R. Granek, Membrane surrounded by viscoelastic continuous media: anomalous diffusion and linear response to force, *Soft Matter* **7**, 5281 (2011).
- [11] E. H. Hauge and A. Martin-Löf, Fluctuating hydrodynamics and Brownian motion, *J. Stat. Phys.* **7**, 259 (1973).
- [12] F. B. Usabiaga, X. Xie, R. Delgado-Buscalioni, and A. Donev, The Stokes–Einstein relation at moderate Schmidt number, *J. Chem. Phys.* **139**, 214113 (2013).
- [13] P. Davy, R. L. Goc, C. Darcel, B. Pinier, J.-O. Selroos, and T. L. Borgne, Structural and hydrodynamic controls on fluid travel time distributions across fracture networks, *Proc. Natl. Acad. Sci. U.S.A.* **121**, e2414901121 (2024).
- [14] B. J. Palmer, J. Chun, J. F. Morris, C. J. Mundy, and G. K. Schenter, Correlation function approach for diffusion in confined geometries, *Phys. Rev. E* **102**, 022129 (2020).
- [15] K. J. Painter, T. Hillen, and J. R. Potts, Biological modeling with nonlocal advection-diffusion equations, *Math. Models Methods Appl. Sci.* **34**, 57 (2024).
- [16] D. Morale, V. Capasso, and K. Oelschläger, An interacting particle system modelling aggregation behavior: from individuals to populations, *J. Math. Biol.* **50**, 49 (2005).
- [17] S.-Y. Ha and E. Tadmor, From particle to kinetic and hydrodynamic descriptions of flocking, *Kinet. Relat. Mod.* **1**, 415 (2008).
- [18] L. D. Landau and E. M. Lifshitz, *Fluid Mechanics*, Course of Theoretical Physics, Vol. 6 (Pergamon Press, 1959).
- [19] D. Bandak, N. Goldenfeld, A. A. Mailybaev, and G. Eyink, Dissipation-range fluid turbulence and thermal noise, *Phys. Rev. E* **105**, 065113 (2022).
- [20] J. M. O. de Zárate and J. V. Sengers, *Hydrodynamic Fluctuations in Fluids and Fluid Mixtures* (Elsevier, 2006).
- [21] P. Español, Stochastic differential equations for nonlinear hydrodynamics, *Physica A* **248**, 77 (1998).
- [22] P. Español, J. G. Anero, and I. Zúñiga, Microscopic derivation of discrete hydrodynamics, *J. Chem. Phys.* **131**, 244117 (2009).
- [23] N. Grimm, J. Baschnagel, A. N. Semenov, A. Zippelius, and M. Fuchs, Stress correlations and stress memory kernels in viscoelastic fluids, *Soft Matter* **21**, 4256 (2025).
- [24] See Supplemental Material at [url will be inserted by publisher] for derivation, simulation details and validations, which includes Ref. [30, 31].
- [25] A. Tamm, M. Caro, A. Caro, G. Samolyuk, M. Klintenberg, and A. A. Correa, Langevin dynamics with spatial correlations as a model for electron-phonon coupling, *Phys. Rev. Lett.* **120**, 185501 (2018).
- [26] F. B. Usabiaga, J. B. Bell, R. Delgado-Buscalioni, A. Donev, T. G. Fai, B. E. Griffith, and C. S. Peskin, Staggered schemes for fluctuating hydrodynamics, *Multiscale Model. Simul.* **10**, 1369 (2012).
- [27] F. B. Usabiaga, L. Pagonabarraga, and R. Delgado-Buscalioni, Inertial coupling for point particle fluctuating hydrodynamics, *J. Comput. Phys.* **235**, 701 (2013).
- [28] F. B. Usabiaga, R. Delgado-Buscalioni, B. E. Griffith, and A. Donev, Inertial coupling method for particles in an incompressible fluctuating fluid, *Comput. Methods Appl. Mech. Eng.* **269**, 139 (2014).
- [29] S. Delong, B. E. Griffith, E. Vanden-Eijnden, and A. Donev, Temporal integrators for fluctuating hydrodynamics, *Phys. Rev. E* **87**, 033302 (2013).
- [30] A. Donev, T. G. Fai, and E. Vanden-Eijnden, A reversible meso-

- scopic model of diffusion in liquids: from giant fluctuations to Fick's law, *J. Stat. Mech.* **2014**, P04004 (2014).
- [31] Y.-H. Shih, G. Wright, J. Andén, J. Blaschke, and A. H. Barnett, cuFINUFFT: a load-balanced GPU library for general-purpose nonuniform FFTs, in *PDSEC2021 workshop of the IPDPS2021 conference* (2021).
 - [32] B. J. Alder and T. E. Wainwright, Decay of the velocity auto-correlation function, *Phys. Rev. A* **1**, 18 (1970).
 - [33] M. H. Ernst, E. H. Hauge, and J. M. J. van Leeuwen, Asymptotic time behavior of correlation functions, *Phys. Rev. Lett.* **25**, 1254 (1970).
 - [34] R. Pastore, A. Coniglio, and M. P. Ciamarra, From cage-jump motion to macroscopic diffusion in supercooled liquids, *Soft Matter* **10**, 5724 (2014).
 - [35] P. Chaudhuri, L. Berthier, and W. Kob, Universal nature of particle displacements close to glass and jamming transitions, *Phys. Rev. Lett.* **99**, 060604 (2007).
 - [36] E. R. Weeks, J. C. Crocker, A. C. Levitt, A. Schofield, and D. A. Weitz, Three-dimensional direct imaging of structural relaxation near the colloidal glass transition, *Science* **287**, 627 (2000).
 - [37] S. Ishino, Y.-C. Hu, and H. Tanaka, Microscopic structural origin of slow dynamics in glass-forming liquids, *Nat. Mater.* **24**, 268 (2025).
 - [38] P. Edera, M. Bantawa, S. Aime, R. T. Bonnecaze, and M. Cloitre, Mechanical tuning of residual stress, memory, and aging in soft glassy materials, *Phys. Rev. X* **15**, 011043 (2025).
 - [39] G. Lois, J. Bławdziewicz, and C. S. O'Hern, Percolation model for slow dynamics in glass-forming materials, *Phys. Rev. Lett.* **102**, 015702 (2009).

Supplemental Material for “Hydrodynamic Trapping of Tracer Particles Induced by Spatially Correlated Noise in Thermal Equilibrium”

Sijie Huang (黄斯杰),^{1,2} Ayush Saurabh,^{1,2} and Steve Pressé^{1,2,3}

¹*Department of Physics, Arizona State University, Tempe, AZ 85287, USA*

²*Center for Biological Physics, Arizona State University, Tempe, AZ 85287, USA*

³*School of Molecular Sciences, Arizona State University, Tempe, AZ 85287, USA*

I. FLUCTUATION-DISSIPATION RELATION

In this section, we derive the fluctuation-dissipation relation (FDR) corresponding to the fluctuating Stokes equation driven by the spatially correlated noise $\hat{\mathcal{Z}}(\mathbf{x}, t)$, as defined in the main text. The fluctuating Stokes equation in Fourier space is a system of decoupled linear Langevin equations

$$\frac{d}{dt}\hat{\mathbf{u}}(\mathbf{k}) = \mathcal{L}\hat{\mathbf{u}} + i\sqrt{2\nu k_B T \rho^{-1}} \mathcal{P}\mathbf{k} \cdot \hat{\mathcal{Z}}, \quad (1)$$

where $\mathcal{P} = \mathbf{I} - \mathbf{k}\mathbf{k}^\top/k^2$ is the Leray projection operator, which projects vectors onto the solenoidal subspace to enforce incompressibility, and $\mathcal{L}(\mathbf{k})$ is the Fourier transform of the linear momentum diffusion operator. For Eq. (1) subject to the uncorrelated noise, the linear diffusion operator recovers the ordinary Laplacian. However, the corresponding operator form in the presence of correlated noise remains to be determined.

Equation (1) can be solved using an integrating factor, leading to the covariance of the Fourier modes as

$$\langle \hat{\mathbf{u}}(\mathbf{k}, t) \hat{\mathbf{u}}^\dagger(\mathbf{k}, t) \rangle = \langle \hat{\mathbf{u}}(\mathbf{k}, 0) \hat{\mathbf{u}}^\dagger(\mathbf{k}, 0) \rangle e^{-\mathcal{L}t} - \frac{\nu k_B T}{\rho} \frac{\mathcal{P}\mathbf{k} \langle \hat{\mathcal{Z}} \hat{\mathcal{Z}}^\dagger \rangle \mathbf{k}^\dagger \mathcal{P}^\dagger}{\mathcal{L}} (1 - e^{-2\mathcal{L}t}), \quad (2)$$

where \dagger denotes the Hermitian conjugate. By definition, \mathcal{P} is real and symmetric, thus $\mathcal{P}^\dagger = \mathcal{P}$. In the long-time limit, all the exponential terms vanish, giving

$$\langle \hat{\mathbf{u}}(\mathbf{k}, t) \hat{\mathbf{u}}^\dagger(\mathbf{k}, t) \rangle = -\frac{\nu k_B T}{\rho} \frac{\mathcal{P}\mathbf{k} \langle \hat{\mathcal{Z}} \hat{\mathcal{Z}}^\dagger \rangle \mathbf{k}^\dagger \mathcal{P}}{\mathcal{L}}, \quad (3)$$

which fixes the equilibrium covariance of the Fourier modes. Substituting the covariance of \mathcal{Z} [Eq. (3) in the main text] into the covariance above and carrying out the algebra yields

$$\langle \hat{\mathbf{u}}(\mathbf{k}, t) \hat{\mathbf{u}}^\dagger(\mathbf{k}, t) \rangle = -\frac{\nu k_B T}{\rho} \frac{k^2 \hat{C}_\ell}{\mathcal{L}} \mathcal{P}, \quad (4)$$

This is the FDR corresponding to Eq. (1) with the correlated noise $\hat{\mathcal{Z}}$.

For uncorrelated noise ($\ell = 0$), $\hat{C}_\ell(\mathbf{k}) = 1$ and $\mathcal{L}(\mathbf{k}) = -\nu k^2$, i.e., the standard Laplacian. Inserting these two expressions into Eq. (4) gives the equilibrium covariance

$$\langle \hat{\mathbf{u}}(\mathbf{k}) \hat{\mathbf{u}}^\dagger(\mathbf{k}) \rangle = \frac{k_B T}{\rho} \mathcal{P}. \quad (5)$$

The resulting covariance is proportional to the projection operator \mathcal{P} , consistent with Ref. [1]. The mean total kinetic energy of the Fourier mode is obtained by taking the trace of the covariance in Eq. (5)

$$\langle |\hat{\mathbf{u}}(\mathbf{k})|^2 \rangle \equiv \text{Tr}[\langle \hat{\mathbf{u}}(\mathbf{k}) \hat{\mathbf{u}}^\dagger(\mathbf{k}) \rangle] = (d-1) \frac{k_B T}{\rho}, \quad (6)$$

where d denotes the dimensionality.

Similarly, for $\ell > 0$, by taking the trace of Eq. (4) and invoking the equipartition condition in Eq. (6), we obtain the modified linear diffusion operator corresponding to the correlated noise $\hat{\mathcal{Z}}$

$$\mathcal{L}(\mathbf{k}) = -\nu k^2 \hat{C}_\ell(k). \quad (7)$$

By the convolution theorem, reverting to the physical space yields the generalized fluctuating Stokes equation

$$\partial_t \mathbf{u} = -\nabla p + \nu \nabla^2 \tilde{\mathbf{u}} + \sqrt{2\nu k_B T \rho^{-1}} \nabla \cdot \mathcal{Z}, \quad (8)$$

where $\tilde{\mathbf{u}}(\mathbf{x}) = \int C_\ell(\mathbf{x}') \mathbf{u}(\mathbf{x} - \mathbf{x}') d\mathbf{x}'$ denotes the correlated velocity.

II. SIMULATION DETAILS

Simulating particle diffusion in fluctuating fluids is inherently a fluid-structure interaction problem. To couple the fluid and particle phases, we employ the inertial coupling method developed in Refs. [2, 3]. The method imposes a no-slip condition on the particle surface, enforcing zero relative velocity between the fluid and the particle and thereby conserving the total momentum of the combined system. If the particles are treated as passive and inertialess—merely advected by the flow without exerting any forces back on the fluid—momentum exchange is absent. Consequently, the fluid-particle equations simplify to

$$\frac{\partial \mathbf{u}}{\partial t} = -\nabla p + \nu \Delta \tilde{\mathbf{u}} + \sqrt{\frac{2\nu k_B T}{\rho}} \nabla \cdot \mathcal{Z}, \quad (9a)$$

$$\frac{d\mathbf{X}}{dt} = \mathbf{v}(\mathbf{X}(t)), \quad (9b)$$

$$\mathbf{v} = \mathcal{J}(\mathbf{X}(t))\mathbf{u}(\mathbf{x}, t) = \int \delta_r(\mathbf{X}(t) - \mathbf{x})\mathbf{u}(\mathbf{x}, t) d\mathbf{x}, \quad (9c)$$

where $\mathbf{X}(t)$ is the particle position, $\mathbf{v}(\mathbf{X}(t))$ its velocity, and δ_r an averaging kernel of width r . The operator $\mathcal{J}(\mathbf{X}(t))$ acts on a continuous field $\mathbf{u}(\mathbf{x})$ and computes its local average at the particle position $\mathbf{X}(t)$. Thus, $\mathbf{v}(\mathbf{X}(t))$ represents the coarse-grained fluid velocity, and Eq. (9b) assumes that the particle is passively advected by this field [4].

In a discrete formulation, spatially white noise must be treated as a spatiotemporal average since the continuum field $\mathcal{W}(\mathbf{x}, t)$ cannot be sampled pointwise in both space and time [see 1, and references therein]. In the actual numerical schemes, the field \mathcal{W} is represented by a set of random numbers \mathbf{W} according to $(\Delta V_f \Delta t)^{-1} \mathbf{W} \leftrightarrow \mathcal{W}$, where ΔV_f is the volume of a computational cell, and Δt is the computational timestep. In practice, the discrete noise \mathbf{W} is sampled using a pseudorandom-number generator.

To ensure that correlated noise reduces to uncorrelated noise ($\mathcal{Z} \rightarrow \mathcal{W}$) as the correlation length vanishes ($\ell \rightarrow 0$), we employ the same spatiotemporal averaging for the correlated field, $(\Delta V_f \Delta t)^{-1} \mathcal{Z} \leftrightarrow \mathcal{Z}$, retaining the prefactor $(\Delta V_f \Delta t)^{-1}$. With this averaging, Eq. (6) yields the equilibrium energy spectrum for the discrete system

$$\langle \hat{\mathbf{u}}(\mathbf{k}) \hat{\mathbf{u}}^*(\mathbf{k}) \rangle = (d-1) \frac{k_B T}{\rho \Delta V_f}, \quad (10)$$

in agreement with Ref. [1].

Unlike the original inertial-coupling method of Refs. [2, 3], where the fluid momentum equation is discretized via a finite-volume scheme, here it is solved directly in Fourier space. Particle trajectories are integrated in time using a midpoint predictor-corrector scheme, while fluid momentum is advanced via the Crank–Nicolson method

$$\frac{\mathbf{X}^{n+\frac{1}{2}} - \mathbf{X}^n}{\Delta t/2} = \mathcal{J}(\mathbf{X}^n)\mathbf{u}^n, \quad (11a)$$

$$\frac{\hat{\mathbf{u}}^{n+1} - \hat{\mathbf{u}}^n}{\Delta t} = \mathcal{L}\left(\frac{\hat{\mathbf{u}}^{n+1} + \hat{\mathbf{u}}^n}{2}\right) + i\sqrt{\frac{2\nu k_B T}{\rho \Delta V_f \Delta t}} \mathcal{P}\mathbf{k} \cdot \hat{\mathbf{Z}}^n, \quad (11b)$$

$$\frac{\mathbf{X}^{n+1} - \mathbf{X}^n}{\Delta t} = \mathcal{J}(\mathbf{X}^{n+\frac{1}{2}})\left(\frac{\mathbf{u}^{n+1} + \mathbf{u}^n}{2}\right). \quad (11c)$$

By the convolution theorem, correlated noise is generated directly in Fourier space by multiplying spatially white noise with the prescribed correlation function

$$\hat{\mathbf{Z}}(\mathbf{k}) = \hat{C}_\ell(\mathbf{k}) \frac{\widehat{\mathbf{W}} + \widehat{\mathbf{W}}^T}{\sqrt{2}}. \quad (12)$$

Averaging $\widehat{\mathbf{W}}$ with its transpose symmetrizes the noise and thereby preserves angular momentum [1]. In this work, for finite correlation length $\ell > 0$, we assume $C_\ell(|\mathbf{x} - \mathbf{x}'|) = \exp[-|\mathbf{x} - \mathbf{x}'|^2/(2\ell^2)]$, and $C_\ell(|\mathbf{x} - \mathbf{x}'|) = \delta(|\mathbf{x} - \mathbf{x}'|)$ for $\ell = 0$. All simulations were performed on GPUs using CuPy.

The particle tracking strategy follows Ref. [4]. The operation $\mathcal{J}(\mathbf{X})$ is divided into two steps: the fluid velocity field is first low-pass filtered in Fourier space, and then the particle velocity is obtained by interpolating the filtered field at the particle position \mathbf{X} . In the present work, the following Gaussian function is used as the filter kernel

$$G_r(\mathbf{x}) = (\pi r^2)^{-d/2} \exp\left(-\frac{\mathbf{x}^2}{r^2}\right), \quad (13)$$

ν	$k_B T / \rho$	L	r	Δx	Δt	t_{end}
$10 \mu\text{m}^2/\text{ms}$	$1 \mu\text{m}^4/\text{ms}^2$	$2\pi \mu\text{m}$	$0.1 \mu\text{m}$	$0.025 \mu\text{m}$	$2 \times 10^{-5} \text{ms}$	200ms

TABLE I. Simulation conditions. ν is the kinematic viscosity, $k_B T / \rho$ is the thermal energy per unit density, L is the domain size, r is the particle radius, Δx is the grid spacing, Δt is the integration timestep and t_{end} is the integration time span. Note that density in two dimensions has units of mass/length².

where r is assumed to be the particle radius. The volume of the particle ΔV_p can be approximated by $\Delta V_p = [\int G_r^2(\mathbf{x}) d\mathbf{x}]^{-1} = (2\pi r^2)^{d/2}$ [2, 3]. The particle volume determined by this Gaussian filter kernel is very close to Peskin’s four-point kernel [2]. After filtering, the interpolation is carried out using a GPU-based non-uniform fast Fourier transform [5].

The fluid-particle system described by Eqs. (9a) and (9b) is solved in a doubly periodic square domain of side length $L = 2\pi \mu\text{m}$, discretized by 256^2 uniform grid points. Simulation conditions are summarized in table I. Fluid properties—viscosity ν and thermal energy per unit density $k_B T / \rho$ —were selected based on numerical constraints, as larger values impose more stringent upper bounds on the integration timestep Δt [3, 6]. The equilibrium thermal velocity for the fluid is determined as $u_{\text{eq}} = \sqrt{k_B T / \Delta m_f} \approx 40.7 \mu\text{m}/\text{ms}$, where $\Delta m_f = \rho \Delta V_f$ denotes the mass of the fluid in a computational cell. The resulting Courant–Friedrichs–Lewy (CFL) numbers are given by

$$\text{CFL}_{\text{inv}} = \frac{u_{\text{eq}} \Delta t}{\Delta x} \approx 0.03 \quad \text{and} \quad \text{CFL}_{\text{vis}} = \frac{\nu \Delta t}{\Delta x^2} \approx 0.33,$$

where CFL_{inv} and CFL_{vis} are the inviscid and viscous CFL numbers, respectively. Both CFL numbers are well below unity, indicating the fluid flow is well-resolved in time [2]. The thermal Reynolds number, $Re = u_{\text{eq}} r / \nu \approx 0.096$ [6], is an order of magnitude smaller than unity, so the flow should be described by the fluctuating Stokes equation.

We seed the flow with 1000 passive tracers, recording their positions every five time steps, corresponding to a sampling interval of 10^{-4}ms . We examine six correlation length-to-particle radius ratios, defined as $\gamma \equiv \ell / r = 0, \frac{1}{4}, 1, 2, 4$, and 6, with particle radius $r = 0.1 \mu\text{m}$ as listed in table I.

III. VALIDATIONS

To validate the simulations, we first examine the fluid phase. At thermal equilibrium, the mean kinetic energy of the fluid is conserved and fluctuates about the expected thermal value, u_{eq}^2 . Figure 1(a) reproduces this behavior with excellent agreement. Satisfaction of the FDR implies energy equipartition among Fourier modes [7, 8], predicting a flat shell-averaged energy spectrum at the equilibrium level described by Eq. (6). Indeed, the spectra in Fig. 1(b) collapse onto this constant line. Moreover, each velocity component should follow the equilibrium Boltzmann distribution

$$P(u_i) = \sqrt{\frac{\Delta m_f}{2\pi k_B T}} \exp\left(-\frac{\Delta m_f u_i^2}{2k_B T}\right). \quad (14)$$

Figure 1(c,d) confirm this prediction: the measured probability density functions (PDF) coincide with the analytic form. Together, energy conservation, equipartition, and the correct velocity statistics demonstrate that the simulations faithfully reproduce the thermal equilibrium of the fluctuating fluids.

We next validate particle diffusion with uncorrelated noise ($\gamma = 0$), which should reproduce classic Brownian behavior. The corresponding results are shown in Fig. 2. Figure 2(a) presents the measured PDF of the particle velocity, approximated by $\mathbf{v}^n = (\mathbf{X}^{n+1} - \mathbf{X}^n) / \Delta t$ [6], together with the equilibrium Boltzmann distribution

$$P(v_i) = \sqrt{\frac{\Delta m_p}{2\pi k_B T}} \exp\left(-\frac{\Delta m_p v_i^2}{2k_B T}\right), \quad (15)$$

where $\Delta m_p = \rho \Delta V_p$ is the particle mass. The agreement confirms that the particles are in thermal equilibrium.

Figure 2(b) and (c) repeat the mean-squared displacement (MSD) and velocity autocorrelation function (VACF) from Fig. 4 of the main text to make this validation self-contained. The MSD, $\Delta X^2(t) = \langle |\mathbf{X}(\tau + t) - \mathbf{X}(\tau)|^2 \rangle$, exhibits the expected crossover from ballistic ($\text{MSD} \propto t^2$) to normal diffusive motion ($\text{MSD} \propto t$). The VACF, $C_v(t) = \langle \mathbf{v}(\tau) \mathbf{v}(\tau + t) \rangle$, displays the hydrodynamic long-time tail t^{-1} between 10^{-3} and 10^{-2}ms , a consequence of hydrodynamic memory effect due to momentum conservation [9, 10]. Beyond this window, finite-domain effects accelerate the decay, consistent with Ref. [6].

The Stokes–Einstein (SE) relation gives the diffusion coefficient of a particle in 2D as [4, 6]

$$D_{\text{SE}} = \frac{k_B T}{4\pi\rho\nu} \ln \frac{L}{ar}, \quad (16)$$

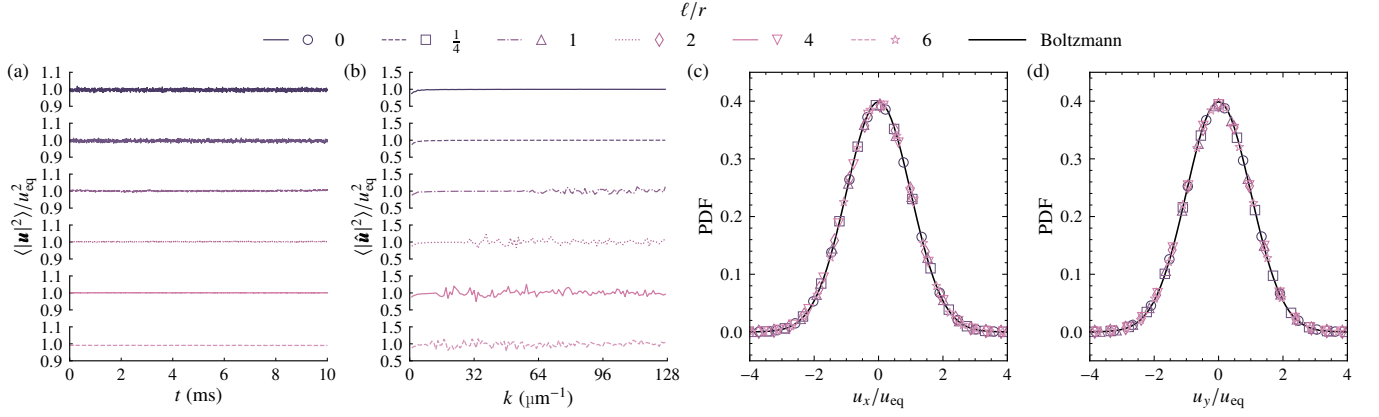


FIG. 1. Confirmation that the fluid phase is at thermal equilibrium for correlation-length-to-particle-radius ratios $\ell/r = 0, \frac{1}{4}, 1, 2, 4$, and 6. (a) Volume-averaged kinetic energy fluctuates around its equilibrium value. (b) Shell-averaged Fourier energy spectra collapse onto the equilibrium equipartition level. (c,d) Probability densities of the velocity components u_x and u_y closely follow the equilibrium Boltzmann distribution. The velocity components are normalized by the thermal velocity u_{eq} .

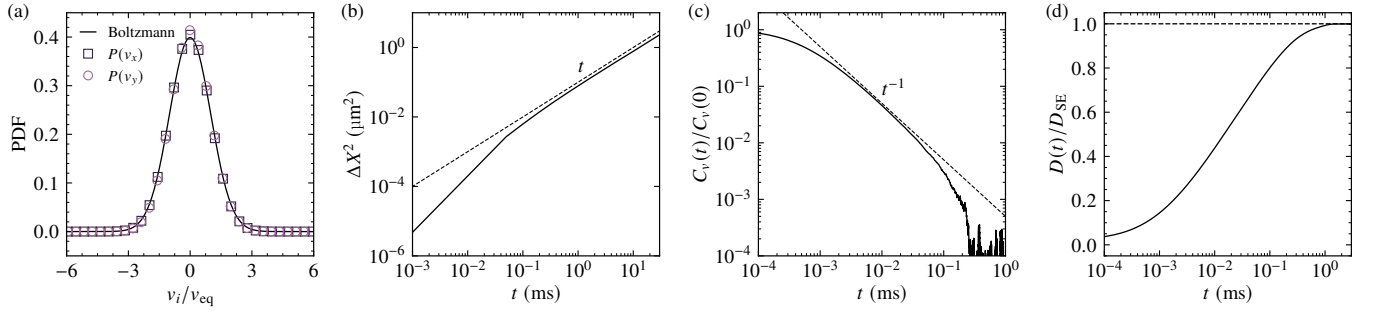


FIG. 2. Confirmation of Brownian diffusion for uncorrelated noise ($\gamma = 0$). (a) Probability densities of the velocity components v_x and v_y collapse onto the equilibrium Boltzmann distribution. The velocity components are normalized by the thermal velocity, $v_{eq} = \sqrt{k_B T / \Delta m_p}$. (b) MSD crossover from ballistic motion, $MSD \propto t^2$, to normal diffusion, $MSD \propto t$. (c) VACF exhibits the hydrodynamic long-time tail $C_v(t) \propto t^{-1}$ between 10^{-3} and 10^{-2} ms. (d) Time evolution of diffusion coefficient $D(t)$ saturates for $t \gtrsim 1$ ms at the Stokes–Einstein value D_{SE} of Eq. (16).

with $a = 5.1$ (close to 5.5 used in Ref. [4]). In the long-time limit, the simulated diffusivity should converge to D_{SE} . The time-dependent diffusivity is approximated by [6]

$$D(n\Delta t) = \frac{\Delta t}{2} C_v(0) + \Delta t \sum_{j=1}^{n-1} \left(1 - \frac{j}{n}\right) C_v(j\Delta t). \quad (17)$$

Figure 2(d) shows that $D(t)$ saturates for $t \gtrsim 1$ ms, and approaches D_{SE} , confirming the expected diffusion rate of the simulated particle.

Taken together—the Boltzmann velocity statistics, the ballistic-to-diffusive MSD crossover, the t^{-1} hydrodynamic tail of the VACF, and the saturation of the diffusivity at the SE value—these results confirm that the simulated particle faithfully reproduces 2D Brownian motion with the correct hydrodynamic coupling.

-
- [1] F. B. Usabiaga, J. B. Bell, R. Delgado-Buscalioni, A. Donev, T. G. Fai, B. E. Griffith, and C. S. Peskin, Staggered schemes for fluctuating hydrodynamics, *Multiscale Model. Simul.* **10**, 1369 (2012).
 - [2] F. B. Usabiaga, L. Pagonabarraga, and R. Delgado-Buscalioni, Inertial coupling for point particle fluctuating hydrodynamics, *J. Comput. Phys.* **235**, 701 (2013).
 - [3] F. B. Usabiaga, R. Delgado-Buscalioni, B. E. Griffith, and A. Donev, Inertial coupling method for particles in an incompressible fluctuating fluid, *Comput. Methods Appl. Mech. Engrg.* **269**, 139 (2014).

- [4] A. Donev, T. G. Fai, and E. Vanden-Eijnden, A reversible mesoscopic model of diffusion in liquids: from giant fluctuations to Fick's law, *J. Stat. Mech.* **2014**, P04004 (2014).
- [5] Y.-H. Shih, G. Wright, J. Andén, J. Blaschke, and A. H. Barnett, cuFINUFFT: a load-balanced GPU library for general-purpose nonuniform FFTs, in *PDSEC2021 workshop of the IPDPS2021 conference* (2021).
- [6] F. B. Usabiaga, X. Xie, R. Delgado-Buscalioni, and A. Donev, The Stokes–Einstein relation at moderate Schmidt number, *J. Chem. Phys.* **139**, 214113 (2013).
- [7] S. Delong, B. E. Griffith, E. Vanden-Eijnden, and A. Donev, Temporal integrators for fluctuating hydrodynamics, *Phys. Rev. E* **87**, 033302 (2013).
- [8] D. Bandak, N. Goldenfeld, A. A. Mailybaev, and G. Eyink, Dissipation-range fluid turbulence and thermal noise, *Phys. Rev. E* **105**, 065113 (2022).
- [9] B. J. Alder and T. E. Wainwright, Decay of the velocity autocorrelation function, *Phys. Rev. A* **1**, 18 (1970).
- [10] M. H. Ernst, E. H. Hauge, and J. M. J. van Leeuwen, Asymptotic time behavior of correlation functions, *Phys. Rev. Lett.* **25**, 1254 (1970).